A Comprehensive Study on the Timing Limits of the TOFPET2 ASIC and on Approaches for Improvements

Vanessa Nadig, Malika Yusopova, Harald Radermacher, David Schug, Bjoern Weissler, Volkmar Schulz, and Stefan Gundacker, *Member, IEEE*

***Abstract*—Novel electronic readout schemes of analog silicon photomultipliers (SiPMs) have shown impressive timing performance of γ-detectors in positron emission tomography (PET). However, transferring these novel concepts to the system level is a key to exploit the improved coincidence time resolution (CTR) in (pre-)clinical imaging. In this study, the commercially available TOFPET2 application-specific integrated circuits (ASICs) from PETsys Electronics S.A. is tested in terms of the best achievable CTR. The measurable CTR limits will be obtained by state-of-the-art high-frequency (HF) readout, minimizing the impact of the electronic front end on the time resolution. We achieved (73 ± 1) ps with the HF readout and (134 ± 10) ps with the TOFPET2 ASIC for a Ce-, and Ca-doped lutetium-oxyorthosilcate (LYSO) crystal of 2 × 2 × 3 mm^2 size. We show that SiPM signal amplification and an effectively reduced TOFPET2 input stage impedance boost the CTR of a 20-mm high LYSO:Ce crystal to 187 ± 8 ps. Our studies also lead to the observation of side peaks in the coincidence time difference spectrum. These peaks are studied in depth and a conclusion on the ASIC for 100-ps PET applications is drawn.**

***Index Terms*—Coincidence time resolution (CTR), front-end electronics, positron emission tomography (PET), radiation detectors for medical applications, timing detectors, time-of-flight positron emission tomography (TOF-PET2) application-specific integrated circuits (ASIC).**

Manuscript received 17 December 2021; revised 14 February 2022; accepted 4 March 2022. Date of publication 11 March 2022; date of current version 3 November 2022. This work was supported by the German Research Association (DFG), under Project 288267690. *(Corresponding authors: Vanessa Nadig; Volkmar Schulz; Stefan Gundacker.)*

This work did not involve human subjects or animals in its research.

Vanessa Nadig, Malika Yusopova, Harald Radermacher, and Stefan Gundacker are with the Department of Physics of Molecular Imaging Systems, Institute for Experimental Molecular Imaging, RWTH Aachen University, 52074 Aachen, Germany (e-mail: vanessa.nadig@pmi.rwth-aachen.de; stefan.gundacker@pmi.rwth-aachen.de).

David Schug and Bjoern Weissler are with the Deparment of Physics of the Molecular Imaging Systems, Hyperion Hybrid Imaging Systems GmbH, 52074 Aachen, Germany.

Volkmar Schulz is with the Department of Physics of Molecular Imaging Systems, Institute for Experimental Molecular Imaging, RWTH Aachen University, 52074 Aachen, Germany, also with the Hyperion Hybrid Imaging Systems GmbH, 52074 Aachen, Germany, also with the Physics Institute III B, RWTH Aachen University, 52074 Aachen, Germany, and also with the Fraunhofer Institute for Digital Medicine MEVIS, 52074 Aachen, Germany (e-mail: volkmar.schulz@pmi.rwth-aachen.de).

Color versions of one or more figures in this article are available at https://doi.org/10.1109/TRPMS.2022.3158704.

Digital Object Identifier 10.1109/TRPMS.2022.3158704

I. Introduction

In TIME-OF-FLIGHT positron emission tomography (TOF-PET), digitizing coincident γ-events with high-precision timestamps is a key to improve the signal-to-noise ratio (SNR) of positron emission tomography (PET) images [1]–[5]. Commonly, fast-decaying scintillators, such as cerium-doped lutetium oxyorthosilicate (LYSO:Ce), and photosensors, such as silicon photomultipliers (SiPMs), which show an excellent single-photon time resolution (SPTR) [5]–[8], are employed in TOF-PET to achieve a high coincidence time resolution (CTR). Recently, ultrafast high-frequency (HF) electronics have been in the focus of many research groups to further improve the CTR. Emerging front-end designs have shown exceptional performance in benchtop experiments and prove that there is a significant contribution of the employed electronics to the overall CTR of current PET systems [8], [9]. Limited by the readout electronics, system-level designs are likely to be a bottleneck when it comes to exploit new avenues in fast timing, such as Cherenkov emission in bismuth germanate (BGO) or halides, e.g., BaF_2, with fast emission in the ultraviolet (UV) range [9]–[12]. Generally, applying advanced readout techniques in a highly integrated form on a system scale, i.e., with a large number of channels, calls for event digitization by application-specific integrated circuits (ASICs) and advanced data handling by field-programmable gate arrays (FPGAs), capable of operating under high-rate conditions. However, limitations imposed by commercially available electronics need to be traced and understood to characterize their origin and propose approaches to overcome them.

A promising candidate for multichannel readout is the TOFPET2 ASIC developed by PETsys Electronics S.A., a 64-channel integrated circuit that can process data rates of up to 600 kcps per individual channel, featuring a three-threshold trigger logic for dark count rejection [13]. The TOFPET2 ASIC consumes a maximum power of 8.2 mW per channel (including signal digitization) and has shown promising performance results in prior studies [14]–[16]. In addition, this ASIC is under investigation by many research groups, making limitations of its electronic front end a subject with a large impact [17]–[21].

In this work, we investigate the timing limits of the ASIC front end by the means of comparing the TOFPET2

performance to an HF readout approach. We further established a combination of the HF readout with the TOFPET2 ASIC with the aim to boost the performance of the ASIC and to take the next essential step to investigate improved signal formation on the system level. Besides the amplification approach, we will exploit the possibility of encoding the signals of a single SiPM with multiple timestamps.

II. Materials and Methods

We established benchtop setups for coincidence measurements with single crystals coupled to individual SiPMs, testing different readout architectures. To establish benchmarks for the timing limits of the scintillators and SiPMs, we first took data with the HF readout concept similar to [8]. Then, we acquired data with the TOFPET2 ASIC evaluation kit to determine the performance in a standard readout mode. The intrinsic timing of the TOFPET2 ASIC was measured as well, connecting one SiPM to two ASIC channels. Afterwards, the electronic signal path prior to the ASIC was modified to investigate the impact of the following modifications made on the CTR: an adapted version of the HF readout circuit from [8] and a multi-timestamp encoding (MTE) approach, both in combination with the TOFPET2 ASIC. The respective setups were placed into a dark chamber where the ambient temperature was regulated to constant 16 °C. A Na-22 point source with an activity of approximately 0.7 MBq was positioned between the two detector pixels in coincidence.

A. Scintillators and Photosensors

We evaluated single detector pixels composed of SiPMs by Broadcom (AFBR-S4N33C013, $3.14 \times 3.14\,\text{mm}^2$, 30 µm SPADs) or Hamamatsu Photonics K.K. (HPK; S14160-3050HS, $3 \times 3\,\text{mm}^2$, 50 μm SPADs) optically coupled to LYSO:Ce crystals (Epic Crystal; $2 \times 2 \times 3\,\text{mm}^3$ and $3 \times 3 \times 20\ \text{mm}^3$) using Cargille Meltmount ($n = 1.539$). In addition, LYSO:Ce,Ca crystals fabricated by Taiwan Applied Crystals (TACs; $2 \times 2 \times 3\ \text{mm}^3$) were used in combination with the aforementioned Broadcom SiPMs. Using a Keithley 2400 Sourcemeter, we acquired I-V curves for the SiPMs used in this work to determine their breakdown voltages and estimate the optimal bias range for coincidence measurements.

B. HF Electronics Featuring Oscilloscope Readout

The state-of-the-art HF readout circuit similar to [8] features a 3 GHz balun transformer (MABA-007159) and two BGA2851 amplifiers for the timing channel and an AD8000 operational amplifier for the energy channel. The timing signal was shaped with decoupling capacitors to minimize baseline shifts. An oscilloscope (Lecroy Waverunner 9404M-MS, bandwidth 4 GHz, 40 GS/s) is used to read out the timing and energy channels, triggering on coincidences (see Fig. 1). We performed bias and threshold scans with all detector configurations as introduced in Section II-A.

C. TOFPET2 ASIC Evaluation Kit

For reference, we acquired data using the TOFPET2 ASIC evaluation kit by PETsys Electronics S.A. (TOFPET2 ASIC

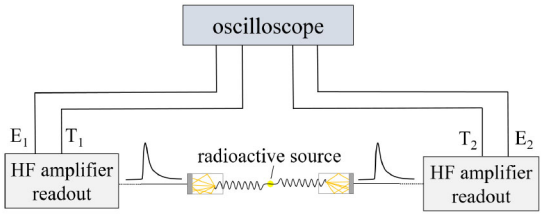

Fig. 1. Schematic assembly of the HF coincidence setup introduced in [8]. The coincidence time difference histogram is computed via the time delay between the two timing channels T_1 and T_2. Energy spectra are acquired via separate energy channels (E_1, E_2).

version 2c) in its standard configuration, employing a sensor front-end board (FEB/S) which enables directly coupling SiPMs to the TOFPET2 ASIC input stage (see Fig. 2, case A). Additional components of the evaluation kit used in this study are two interface front-end boards (FEB/I) connecting the ASIC to the motherboard (FEB/D_v2) via flexible HQCD cables, an HV-DAC mezzanine board generating the SiPM bias voltage, and a Gigabit Ethernet (GbE) board routing data to the lab computer. After calibrating the channel baselines, time-to-digital converters (TDCs) and charge-to-digital converters (QDCs) using the calibration routine provided with the evaluation kit software, we performed bias and threshold scans with a reduced input stage impedance of approximately 11 Ω (by setting fe_ib1 = 0 in the ASIC configuration file) and with default trigger configuration (three-threshold trigger logic). The second timing threshold vth_t2 = 20 and the energy threshold vth_e = 15 are kept constant, while the first timing threshold vth_t1 is varied using a least significant bit (lsb) value of 6.66 mV. The ASIC is operated in the charge-to-digital converting (QDC) mode, determining the signal energy via signal integration over a period of 290 ns. Using the convert_raw_to_singles_method implemented by PETsys Electronics S.A., acquired raw data are converted to single hit information, each with a timestamp, energy value, and channel-ID.

D. Intrinsic Timing of TOFPET2 ASIC

To measure the intrinsic timing performance of the TOFPET2 ASIC, one SiPM was connected to two channels on the same ASIC as depicted in Fig. 3 via a custom adapter board. This measured intrinsic timing performance ($\text{CTR}_{\text{intrinsic}}$) mainly consists of the TDC resolution and the contribution of the front end. If we consider that the $\text{CTR}_{\text{intrinsic}}$ is losely correlated to the timing performance of the employed SiPM-crystal configuration, which we can measure via HF readout, i.e., (CTR_{HF}), the contributions add up quadratically and the CTR measured in coincidence experiments with the TOFPET2 ASIC ($\text{CTR}_{\text{TOFPET2}}$) should correspond to:

$$\text{CTR}_{\text{TOFPET2}} = \sqrt{\text{CTR}_{\text{HF}}^2 + \text{CTR}_{\text{intrinsic}}^2} \tag{1}$$

To measure the intrinsic timing performance of the TOFPET2 ASIC, using the custom-designed MTE board, a Broadcom AFBR-S4N33C013 SiPM coupled to an LYSO:Ce crystal (EPIC, $2 \times 2 \times 3\ \text{mm}^3$) was connected to two channels of the same ASIC.

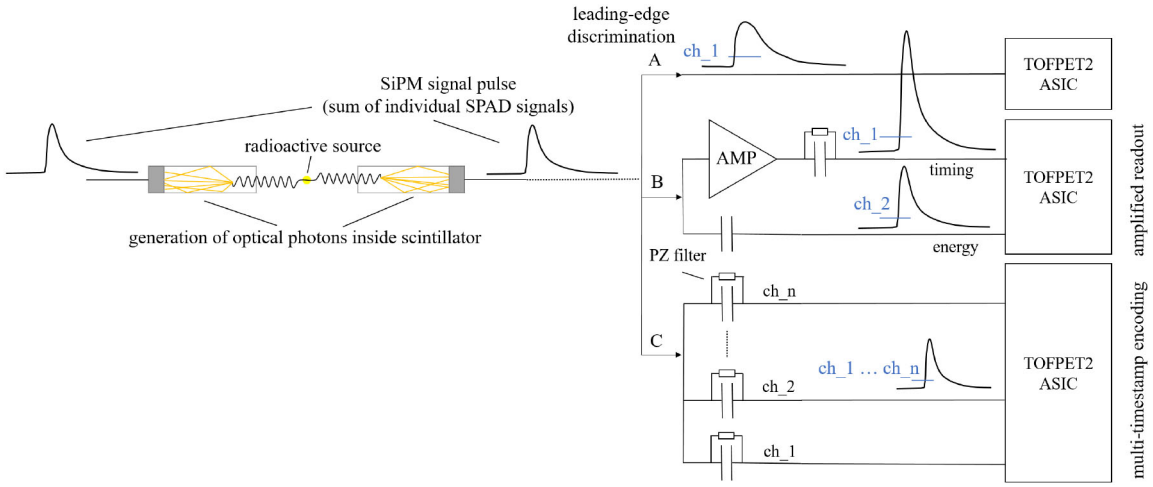

Fig. 2. Schematic drawing of the coincidence setups employing the TOFPET2 ASIC evaluation kit as bought from PETsys Electronics S.A. and custom front-end designs replacing the PETsys FEB/S. (A) Leading-edge discrimination with a single threshold on SiPM signal and the default PETsys hardware. (B) Leading-edge discrimination with a single threshold on amplified SiPM signal in the timing and energy branch. This corresponds to the amplified readout in combination with the TOFPET2 ASIC. (C) MTE using up to n channels with the same trigger thresholds.

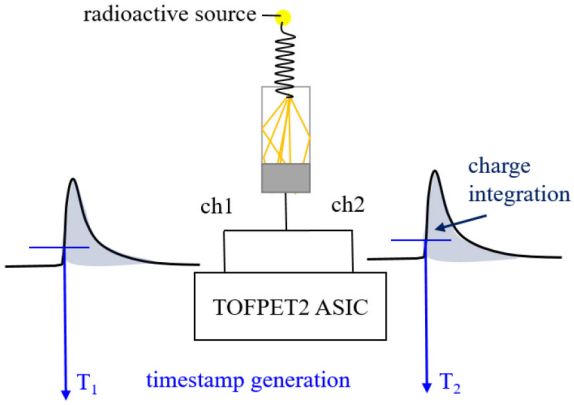

Fig. 3. Schematic drawing of the setup used to measure the intrinsic timing performance of the TOFPET2 ASIC: One SiPM is connected to two channels of the same ASIC. The threshold is configured to the same level in both channels.

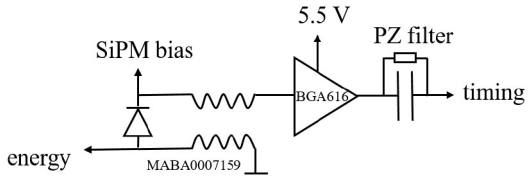

Fig. 4. Simplified schematic of the amplified readout circuit. Circuit was adapted from [8].

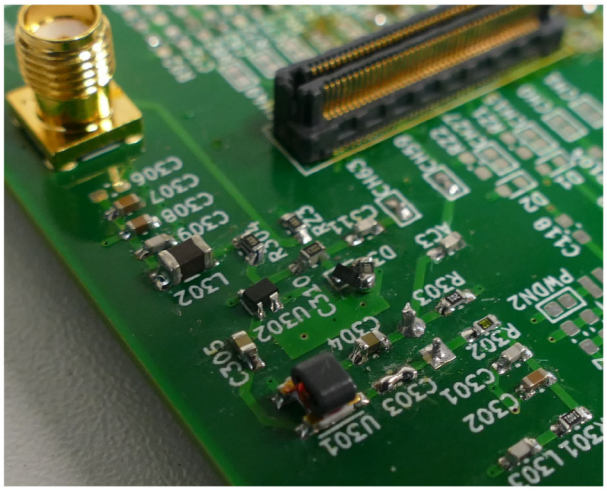

Fig. 5. Picture of the FEB/S replacement board schematically shown in Fig. 2. The board comprises several test circuits, such as the amplifier circuit [Fig. 2(B)] and the MTE circuit [Fig. 2(C)]. The image shows the amplifier circuit. The photosensor is connected from the backside of the board.

E. Amplified Readout With TOFPET2 ASIC

Inspired by an HF readout presented in [8], we modified the circuit to be adapted to the TOFPET2 ASIC input stage (see Fig. 4). For the timing channel, the differential SiPM signal extracted via a transformer (MABA-007159, MACOM) is amplified by a broadband amplifier (BGA616; Infineon Technologies) operated at a supply voltage of 5.5 V, drawing a current of 35 mA and hence adding an additional power consumption of 193 mW per amplified readout channel. Afterward, the signal is pole-zero (PZ) filtered employing a serial capacitor (270 pF) and a resistor (400 Ω) in parallel. PZ filters are used to obtain short signal pulses with a fast-rising edge and prevent pile-up effects [22]. The energy information is extracted via a separate channel to maintain an acceptable energy resolution that does not suffer from filtering the signals. The number of amplifiers in the timing channel was reduced to one to reduce the amplification factor and meet the requirement of a signal with a positive input polarity for the TOFPET2 ASIC in version 2c. The signal of the timing branch is clipped by means of a fast Schottky diode to avoid exceeding the absolute maximum ratings of the TOFPET2 ASIC input stage. The operational amplifier in the energy channel was omitted completely. We replaced the FEB/S by the custom-designed amplified readout circuit, establishing a connection to the ASIC front-end board (FEB/A) housing the TOFPET2 ASIC (see Figs. 2(B)

and 5). Using the custom-designed board, the signal height of a single SPAD after amplification and filtering before the ASIC input was measured. The average height of the signal amplitude was computed as the mean maximum amplitude for the acquired waveforms. Afterwards, we conducted dark count scans using a technique also shown in [15] and [23] for a reference channel as well as the HF timing and energy channel with the trigger logic reconfigured to only trigger on the first discriminator threshold. When plotting the dark count rate (DCR) over the configured trigger threshold, these scans link the trigger level to the number of fired SPADs, visible as pedestals in the plot, after pre- and post-amplification of the signal inside the ASIC. With this, the effective signal amplification factor due to the employed BGA616 amplifier was estimated.

Afterward, bias and threshold scans were performed to assess the timing performance of the circuit in coincidence experiments. Acquired hits in the timing and energy channel are clustered within a period of 5 ns, assigning the timestamp of the timing channel and the energy value of the energy channel to the resulting event.

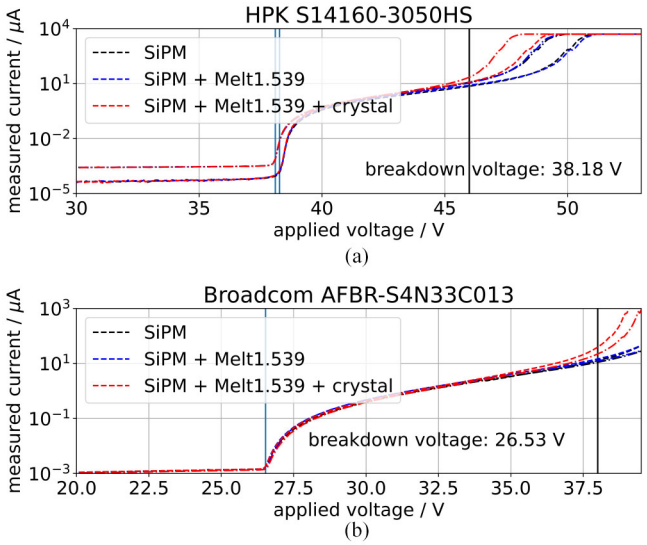

Fig. 6. I-V curves for the different SiPMs and LYSO:Ce $2 \times 2 \times 3$ mm^3 manufactured by Epic Crystals. The optical coupling was realized using Cargille Meltmount ($n = 1.539$). (a) HPK S14160-3050HS. (b) Broadcom AFBR-S4N33C013.

F. Multi-Timestamp Encoding

MTE has recently been investigated in simulation and neural network studies and has been considered for application on the PET system level. It allows for timestamp averaging and time walk corrections based on the rising edge of the acquired signals [11], [24]–[27]. Optionally combined with PZ filters, MTE is expected to reduce the effective input impedance seen by the SiPM, ultimately resulting in a faster signal decay and hence reduced baseline shifts. In this study, we replaced the FEB/S by a custom-designed MTE circuit, establishing a connection to the ASIC front-end board (FEB/A) housing the TOFPET2 ASIC [see Fig. 2(C)] and allowing to connect one SiPM to several ASIC channels to generate multiple timestamps for the same signals. Since the TOFPET2 ASIC allows for individual channel configuration, the leading-edge threshold applied to each channel was set to the same level to average timestamps [see Fig. 2(C)]. The connection was realized either directly (DC coupling) or via using a PZ filter. Using Broadcom AFBR-S4N33C013 SiPMs in combination with LYSO:Ce,Ca crystals (TAC; $2 \times 2 \times 3$ mm^3), between one and six ASIC channels were connected to one SiPM channel. The performance of each configuration was evaluated in coincidence measurements, applying different bias voltages and thresholds. The same clustering algorithm as for the amplified readout is applied to events encoded with multiple timestamps using a cluster window of 15 ns, assigning either the first or the mean timestamp to the resulting cluster. In this work, only results for averaging the timestamps are reported, since picking the first timestamp generally resulted in worse CTRs. The energy of the event is determined from only one of the connected channels. We applied a skew correction to the timestamps with respect to one reference channel on each board to account for the different electrical signal path lengths of multiple ASIC channels connected to one SiPM.

G. Data Processing

Acquired data were processed using dedicated algorithms for coincidence matching. The position of the photopeak in the raw energy value spectrum of each detector is determined. Events with an energy value within 3σ around the photopeak in the raw energy value spectrum of the respective channel are considered for a coincidence search. The coincidence search is performed applying a coincidence window of 7.5 ns. The CTR is computed as full width at half maximum (FWHM) of the Gaussian fit to the peak in the time difference histogram.

III. Results

A. Scintillators and Photosensors

The acquired I-V curves are shown in Fig. 6 with and without optical coupling to a scintillator for the case of short LYSO:Ce crystals (EPIC; $2 \times 2 \times 3$ mm^3). The blue- and black-dashed curves overlap as adding an optical coupling agent does not significantly change the external crosstalk probability of the SiPM. A scintillator mounted on top, however, changes this behavior (see red-dashed curves in Fig. 6) due to the light reflection given by the Teflon wrapping. For the Broadcom SiPMs, a breakdown voltage of 26.53 V could be determined [see blue line in Fig. 6(b)]. For the Hamamatsu SiPMs, the breakdown voltage was slightly different for the two SiPMs used and was, therefore, averaged to 38.18 V [see blue lines in Fig. 6(a)]. From the I-V curves in Fig. 6, we can furthermore deduce that HPK and Broadcom SiPMs will be operable up to a certain bias voltage, before an increased correlated noise prevents the operation of the SiPM. For HPK SiPMs, this limit is located at around 46 V, indicated by the steep rise of the measured current above a level of 100 µA [see black line in Fig. 6(a)]. For Broadcom SiPMs, the limit will be at about 38 V [see black line in Fig. 6(b)].

TABLE I
CTR ACHIEVED WITH THE REFERENCE ELECTRONICS (TOFPET2 ASIC EVALUATION KIT) AND THE AMPLIFIED READOUT CIRCUIT IN COMBINATION WITH THE TOFPET2 ASIC AT SIPM OVERVOLTAGE OF APPROX. 7.5 V. THE REPORTED VALUES ARE MEAN VALUES AND STANDARD DEVIATIONS COMPUTED OUT OF FIVE INDIVIDUAL MEASUREMENTS

SiPM	Scintillator	CTR_{HF} / ps	$CTR_{TOFPET2}$ / ps	$CTR_{TOFPET2+HF}$ / ps	CTR_{MTE} / ps
HPK S14160-3050HS	LYSO:Ce (EPIC) 3×3×20 mm^3	146 ± 2	200 ± 1	191 ± 2	n.a.
	LYSO:Ce (EPIC) 2×2×3 mm^3	91 ± 2	141 ± 2	136 ± 3	n.a.
Broadcom AFBR-S4N33C013	LYSO:Ce (EPIC) 3×3×20 mm^3	132 ± 2	203 ± 1	187 ± 8	n.a.
	LYSO:Ce (EPIC) 2×2×3 mm^3	82 ± 2	142 ± 4	128 ± 4	n.a.
	LYSO:Ce,Ca (TAC) 2×2×3 mm^3	73 ± 1	134 ± 10	n.a.	118 ± 5

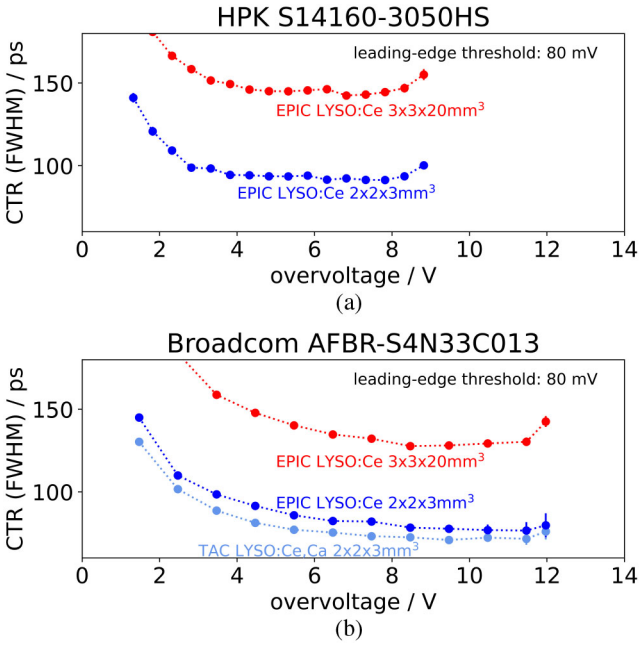

Fig. 7. Coincidence timing resolution of the presented SiPM-crystal configurations achieved with the HF SiPM readout introduced in [8] and digitization via an oscilloscope (Lecroy Waverunner 9404M-MS, bandwidth 4 GHz, 40 GS/s). The leading-edge threshold was configured to 80 mV (about half the height of a single-SPAD signal) for all SiPM bias voltages. (a) HPK S14160-3050HS. (b) Broadcom AFBR-S4N33C013.

B. HF Electronics Featuring Oscilloscope Readout

Using similar electronics as in [8], we determined the performance limits of the present scintillators and SiPMs as a reference. With a leading-edge threshold, which was optimized via the conducted threshold scans, in the range of half the single-SPAD amplitude, the measurements yielded a CTR of (73 ± 1) ps for LYSO:Ce,Ca crystals (2 × 2 × 3 mm^3) coupled to Broadcom SiPMs (see Table I and Fig. 7). LYSO:Ce crystals (2 × 2 × 3 mm^3) in combination with Broadcom SiPMs and Hamamatsu SiPMs achieved worse CTRs, (82 ± 2) and (91 ± 2) ps, respectively. Longer scintillator crystals adapted to the cross section of the SiPM (3 × 3 × 20 mm^3) deteriorated these values to CTRs of (132 ± 2) and (146 ± 2) ps with Broadcom and HPK, respectively (see Table I and Fig. 7).

C. Standard Readout With TOFPET2 ASIC

Applying the TOFPET2 ASIC as electronic front end and coupling a small LYSO:Ce,Ca crystal (TAC; 2 × 2 × 3 mm^3) to Broadcom AFBR-S4N33C013 SiPMs yielded a CTR of (134 ± 10) ps. Using standard LYSO:Ce crystals (EPIC; 2 × 2 × 3 mm^3) results in a CTR of (141 ± 2) ps for HPK S14160-3050HS SiPMs and (142 ± 4) ps for Broadcom AFBR-S4N33C013 SiPMs. For 3 × 3 × 20 mm^3 LYSO:Ce crystals from the same manufacturer, the CTR was (200 ± 1) and (203 ± 1) ps for HPK and Broadcom SiPMs. Table I shows these values in comparison to the CTR achieved with the HF readout circuit.

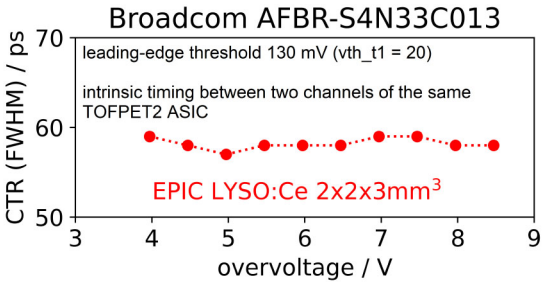

Fig. 8. Intrinsic CTR of the TOFPET2 ASIC measured with a Broadcom AFBR-S4N33C013 SiPM coupled to an LYSO:Ce crystal (EPIC, 2 × 2 × 3 mm^3) connected to two specific ASIC channels of the same ASIC using the MTE circuit. The leading-edge threshold was configured at approximately 130 mV (vth_t1 = 20).

D. Intrinsic Timing of the TOFPET2 ASIC

With a Broadcom AFBR-S4N33C013 SiPM coupled to an LYSO:Ce crystal (EPIC; 2 × 2 × 3 mm^3) connected to two channels of the same ASIC, the intrinsic CTR of the TOFPET2 ASIC was measured to be on average 58 ps at a threshold of vth_t1 = 20 over the whole bias range scanned (see Fig. 8).

E. Amplified Readout With TOFPET2 ASIC

Adding differential SiPM readout, an amplification stage and a PZ filter between the SiPM and the TOFPET2 ASIC resulted in resolving single-photon triggers and a significant CTR improvement to values below 200 ps for crystals with 20 mm length.

1) Resolving Single-Photon Triggers: Single-SPAD waveforms were acquired after the amplification with the BGA616 and before the ASIC input stage using an oscilloscope (Keysight Infiniium DSOS204a, bandwidth 2.1 GHz, 20 GS/s). Employing the BGA616 amplifier, the single-SPAD signal amplitude could be increased to 1.4 mV for Broadcom AFBR-S4N33C013 SiPMs and to 2.8 mV for HPK S14160-3050HS SiPMs (see Fig. 9).

With the TOFPET2 ASIC configured to a single-threshold timing trigger, this results in single-photon triggers being

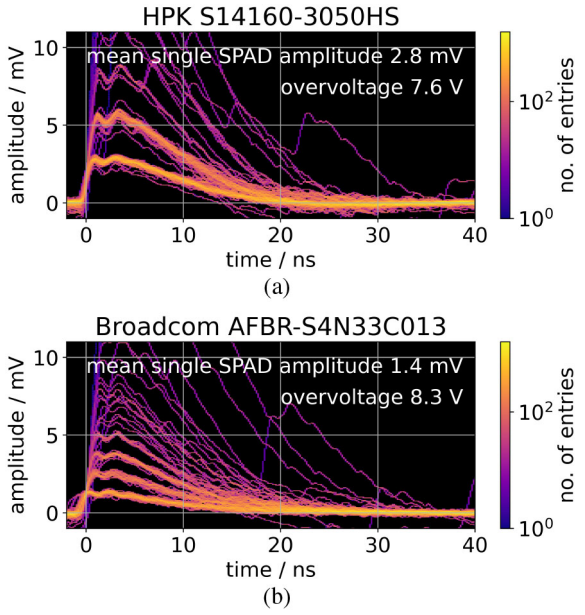

Fig. 9. Selected waveforms representing single SPAD breakthroughs acquired with the adapted amplified readout in combination with the TOFPET2 ASIC. The signals were recorded after the amplification with the BGA616 operated at 5.5 V and before the ASIC input stage (Rin = 11 Ω) with an oscilloscope (Keysight Infiniium DSOS204a, bandwidth 2.1 GHz, 20 GS/s). (a) HPK S14160-3050HS. (b) Broadcom AFBR-S4N33C013.

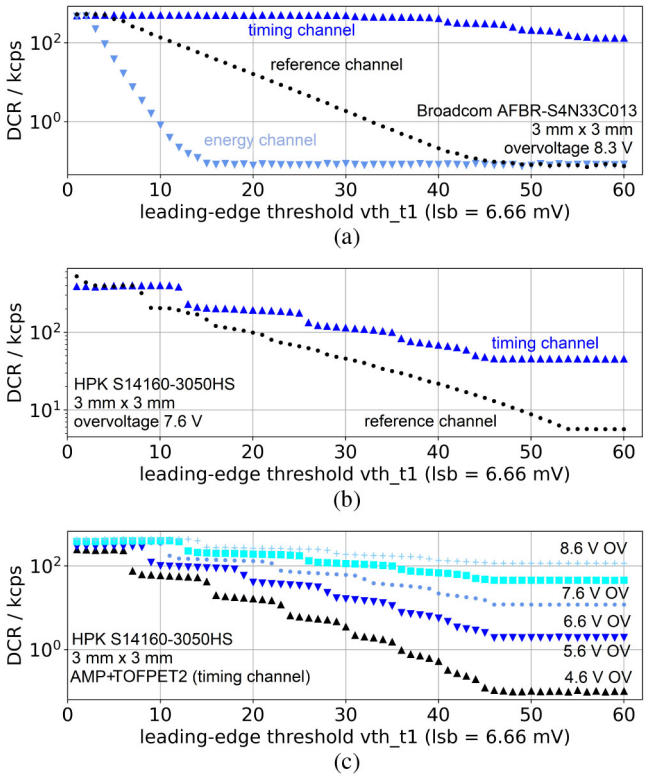

Fig. 10. DCR at various leading-edge thresholds with the discriminator configured at a step width of 6.66 mV. (a) DCR acquired with Broadcom AFBR-S4N33C013 SiPMs for the reference, timing and energy channel at an overvoltage of 8.3 V. (b) DCR acquired with HPK S14160-3050HS SiPMs for the reference and timing channel at an overvoltage of 7.6 V. (c) DCR acquired with HPK S14160-3050HS SiPMs for the amplified readout channel, i.e., the timing channel, at various overvoltages, ranging from 4.6 to 8.6 V.

resolved as pedestals in the staircase plot for Broadcom AFBR-S4N33C013 SiPMs [see Fig. 10(a)] that could not be resolved with the reference electronics at the given discriminator configuration (lsb value 6.66 mV). The fast drop of the DCR for the energy channel is expected due to AC coupling (100 nF) to the ASIC input stage [see Fig. 10(a)]. For HPK S14160-3050HS SiPMs, the single-photon pedestals could already be resolved before amplification due to the larger SPAD size, but are now stretched over the configured threshold range [see Fig. 10(b) and (c)]. From the pedestals in the staircase plot for HPK S14160-3050HS SiPMs, one can deduce that the effective amplification factor is about 3. It has to be noted that the signals are further amplified and shaped by the ASIC's pre- and post-amplifier, thus a single-SPAD amplitude, i.e., the length of a single-SPAD pedestal, in Fig. 10 does not correspond to the amplified single-SPAD signal shown in Fig. 9, which was measured at the BGA616 output before the ASIC.

2) CTR Improvement: The CTR was improved using the amplified readout circuit in combination with the TOFPET2 ASIC compared to using the TOFPET2 ASIC with the electronics shipped with its evaluation kit and the SiPMs from both Broadcom and HPK. While higher leading-edge thresholds yielded improved CTRs, the adapted circuit performed equal to or worse than the reference electronics in many cases for lower leading-edge thresholds (see Fig. 11). This is expected since the signal range we are triggering on is scaled by approximately a factor of 3 due to the amplification. The additional deterioration at very low thresholds for measurements with the amplifier could be due to a higher electronic noise caused by the amplifier.

For HPK S14160-3050HS, the CTR improved from (141 ± 2) to (136 ± 3) ps in the case of 2 × 2 × 3 mm^3 LYSO:Ce crystals. For Broadcom AFBR-S4N33C013, the CTR improved from (142 ± 4) to (128 ± 4) ps in the same case. For crystals of 20 mm length (EPIC; LYSO:Ce 3 × 3 × 20 mm^3), the CTRs improved below 200 ps for both SiPMs types, with Broadcom SiPMs outperforming HPK and achieving a CTR of (187 ± 8) ps (see Table I). The improvement was observed to be generally larger for Broadcom AFBR-S4N33C013 SiPMs. Since these SiPMs feature a higher DCR than the ones from HPK and are thus more prone to baseline shifts and pile-up effects, the employed PZ filter was probably more effective in this configuration, which leads to a larger CTR improvement. It has to be noted that the improvements reported and depicted in Fig. 11 compare the performance of the two circuits, i.e., the TOFPET2 ASIC as commercially available and the adapted circuit from [8] in combination with the TOFPET2 ASIC, for their individual optimal overvoltages and not at the same overvoltage. However, as can be seen from Fig. 7, we can conclude that the slight shift in overvoltages does not significantly alter the intrinsic performance of the SiPM and crystal configuration.

F. Multitimestamp Encoding

Connecting an increasing number of TOFPET2 ASIC channels to one SiPM results in an improved timing performance of Broadcom AFBR-S4N33C013 SiPMs coupled to LYSO:Ce,Ca

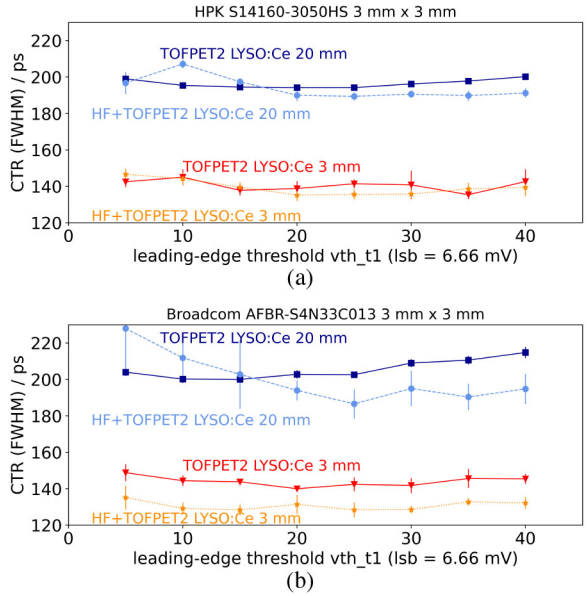

Fig. 11. Performance of different scintillators and SiPMs with the TOFPET2 ASIC and with the TOFPET2 ASIC in combination with amplified readout. The overvoltage was set with respect to the optimum performance of each circuit. (a) HPK S14160-3050HS. For the measurements with the TOFPET2 ASIC, an overvoltage of 6.8 V was applied. For measurements in combination with the amplified readout, an overvoltage of 7.6 V was applied. (b) Broadcom AFBR-S4N33C013. For the measurements with the TOFPET2 ASIC, an overvoltage of 7.5 V was applied. For measurements in combination with the amplified readout, an overvoltage of 8.3 V was applied.

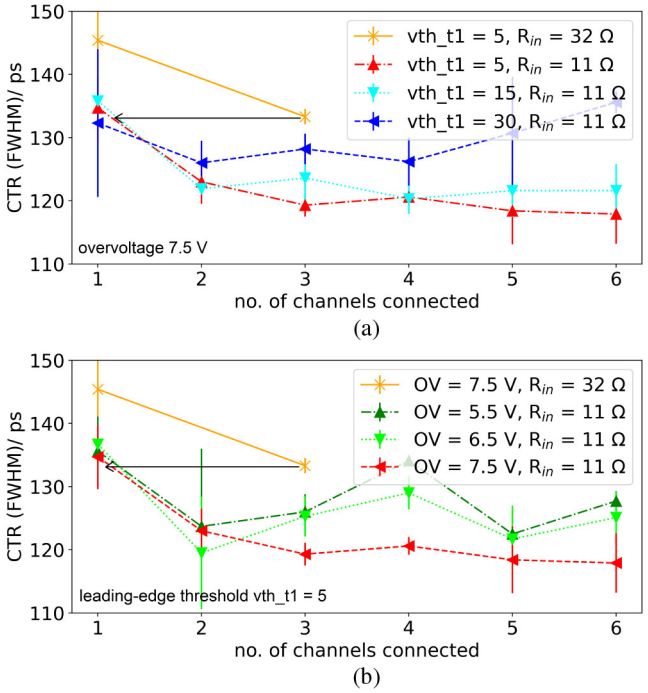

Fig. 12. CTR of Broadcom AFBR-S4N33C013 SiPMs coupled to LYSO:Ce,Ca crystals ($2 \times 2 \times 3$ mm^3) with the MTE circuit connected to the TOFPET2 ASIC. (a) CTR depending on the number of channels connected and the leading-edge threshold (same threshold configured for all channels) at an overvoltage of 7.5 V. (b) CTR depending on the number of channels connected and the overvoltage as parameter. The leading-edge threshold was set to 33 mV (vth_t1 = 5) for all connected channels.

crystals ($2 \times 2 \times 3$ mm^3) (see Fig. 12). When configuring different leading-edge thresholds while maintaining a constant overvoltage, the CTR clearly benefits from MTE in the case of triggering on lower leading-edge thresholds, while at higher leading-edge thresholds there is only a slight improvement. For five and six channels being connected, even a deterioration was observed for higher leading-edge thresholds [see Fig. 12(a)], which is probably caused by the much lower signal amplitude for a higher number of channels being connected. For varying the overvoltage at constant leading-edge thresholds, a similar effect is observed with the timing performance benefiting more from multiencoded timestamps at higher overvoltages [see Fig. 12(b)]. Overall, the best CTR achieved was (118 ± 5) ps at an overvoltage of 7.5 V, a leading-edge threshold of 33 mV (vth_t1 = 5) and with five to six ASIC channels connected to one SiPM. Since higher overvoltages are associated with an increased probability for pile-up effects, baseline shifts, and triggering on dark counts, it seems that the connection of multiple channels stabilizes this regime. Furthermore, when acquiring data with the default input stage impedance of 32 Ω and connecting three instead of one channel, it can be seen that the CTR is improved to the level of a measurement with an input stage impedance of 11 Ω (see Fig. 12, orange curves), which is approximately 1/3 of the default input stage impedance. This supports the aforementioned assumption that the reduced input impedance is the main driver of the CTR improvement, most likely due to a reduced baseline shift.

G. Observation of Novel Side Peaks in Coincidence Time Difference Spectra

Pushing the timing performance of the TOFPET2 ASIC, the coincidence time difference spectra acquired with the reference electronics, i.e., the TOFPET2 ASIC evaluation kit, revealed additional peaks [see Fig. 13(a)]. The outermost peaks located at around ± 5600 ps have been characterized in prior studies and correspond to the so-called satellite peaks, which are generated by falsely assigned timestamps in the trigger circuit due to the configurable delay of the first timing trigger [14]. They are provoked by high overvoltages and low trigger thresholds, meaning in Fig. 13(a) they are suppressed due to a high vth_t1. The four peaks close to the main peak, however, have been newly observed and are to the best of our knowledge not reported in the literature. These peaks are observed for versions 2b and 2c of the TOFPET2 ASIC. Results reported here have been produced with ASIC version 2c. Other ASIC versions have not been the subject of these investigations. The peaks might only become apparent in semi-logarithmic visualization, as their amplitude is small compared to the main peak, or even vanish completely in the tails of broader time difference distributions. Reaching CTRs in the order of 130 ps revealed them. Operating the SiPM with a higher bias voltage or using the amplified readout circuit in combination with the TOFPET2 ASIC increases the peak amplitude [see Fig. 13(b)]. Especially the second-order peaks become more pronounced. In order to study these side peaks in more detail, we report

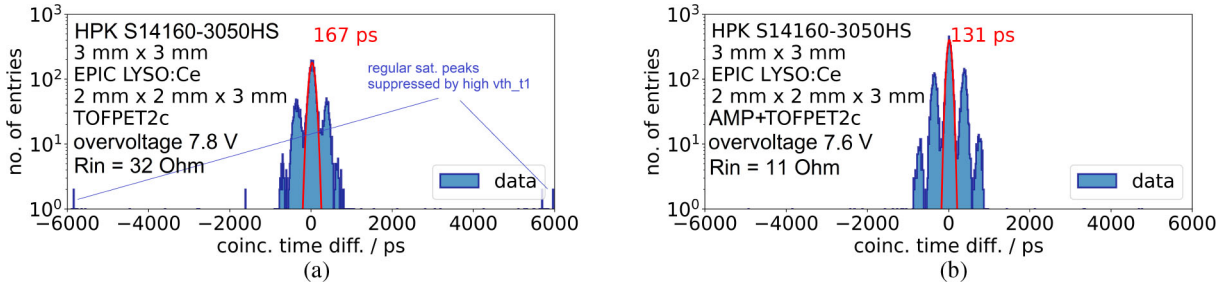

Fig. 13. Coincidence time difference spectra revealing multiple side peaks. The spectra were acquired with HPK S14160-3050HS SiPMs with a trigger threshold of 130 mV (vth_t1 = 20). (a) Reference electronics as bought from PETsys Electronics S.A. at an overvoltage of 7.8 V with default configuration (R_{in} = 32 Ω). (b) Amplified readout in combination with the TOFPET2 ASIC at an overvoltage of 7.6 V.

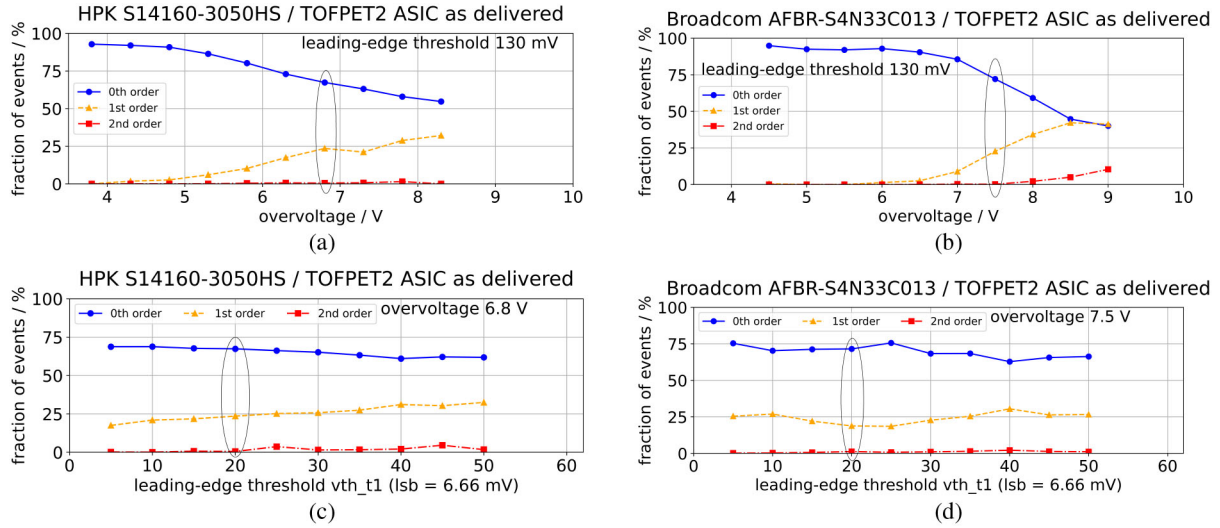

Fig. 14. Side-peak occurrence in coincidence time difference spectra depending on overvoltage an threshold settings. The plots show measurements with the default hard and software configuration of the PETsys TOFPET2 ASIC for a range of applied SiPM bias voltages at a leading-edge threshold of approx. 130 mV (vth_t1 = 20) [(a) and (b)] and leading-edge thresholds at an overvoltage of 6.8 V (HPK) and 7.5 V (Broadcom), respectively [(c) and (d)]. Data were acquired with (a) and (c) HPK S14160-3050HS. (b) and (d) Broadcom AFBR-S4N33C013. Data acquired with the same settings for each SiPM type are highlighted with black circles.

the fraction of events contributing to the side peaks plotted against the SiPM overvoltage in Fig. 14(a) and (b) for PETsys hardware only and default ASIC configuration. Here, the visible peaks in the coincidence time difference spectra were each fitted with a Gaussian. The fraction of events in a 2σ-environment of the mean value of each peak was computed with regard to the total number of coincidences. It can be seen that the first- and second-order peaks are not present for lower overvoltages, but start to appear and gain in amplitude with increasing overvoltage, while the fraction of events contributing to these peaks stays almost constant over the whole investigated threshold range [Fig. 14(c) and (d)]. It has been checked that the number of coincidences remained approximately constant for the investigated settings, confirming that the events in the peaks are true coincidences and not duplicates from other acquired coincidences. The side peaks occur earlier, i.e., at a lower overvoltage for HPK S14160-3050HS SiPMs, which generally produce larger signals than Broadcom AFBR-S4N33C013 due to their larger SPADs [see Figs. 9 and 14(a) and (b)]. At higher overvoltage, up to 40 % of the acquired coincidences are affected by a falsely generated timestamp for Broadcom AFBR-S4N33C013 SiPMs. The fraction of events affected is generally lower for HPK S14160-3050HS SiPMs [see Fig. 14(a)]. In Fig. 14(c), also a threshold dependency becomes apparent in contrast to Broadcom AFBR-S4N33C013 SiPMs see Fig. 14(d)]. Due to the dependency on the overvoltage, we conclude that these peaks might be linked to the height of the signal that is routed into the ASIC input stage rather than the steepness of the signal's rising edge. This is supported by the fact that the usage of smaller capacitors in the PZ filters decreases the side-peak amplitude. The investigation on the exact reason for the generation of these peaks is ongoing. As shown in Fig. 15, a possible workaround is to reconfigure the TOFPET2 trigger circuit to a single-threshold trigger in the energy branch, which results in triggering on a much higher leading-edge threshold (lsb value is increased by a factor of 8). This comes at the cost of timing performance, yielding a CTR that is 30 ps worse.

Once $n \geq 2$ ASIC channels are connected to one SiPM using the MTE approach, the newly observed side peaks vanish from the coincidence time difference histogram, although at least the first-order peaks were present for $n = 1$ ASIC channels connected to one SiPM. We assume that this might be due to two superposing effects, where the first one would

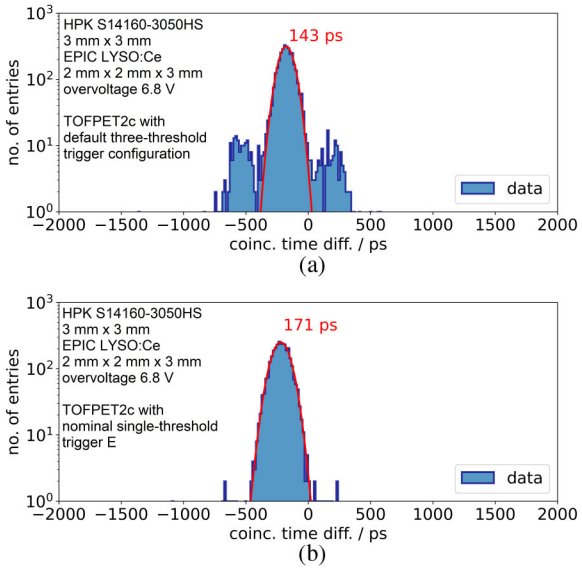

Fig. 15. Coincidence time difference spectra acquired with the standard PETsys TOFPET2 hardware and HPK S14160-3050HS SiPMs coupled to LYSO:Ce crystals (EPIC; 2 × 2 × 3 mm^3) at an overvoltage of 6.8 V. (a) Default trigger logic configuration. (b) Triggering on a single-threshold trigger in the energy branch of the ASIC channel. Apart from that, the same settings as in (a) have been used.

be hardware driven and the second one would processing driven: on one hand, reducing the input stage impedance by connecting multiple ASIC channels leads to a faster signal decay and furthermore splits up the current signal, reducing the signal amplitude. As the appearance of the side peaks is strongly dependent on the signal height, they will not be visible anymore. On the other hand, assuming that the false timestamp assignment occurs at a rate that only one of the connected ASIC channels is affected at a time, timestamp averaging in data processing would result in certainly shifting this timestamp toward the main peak. Thus, the applied processing method could probably also contribute to diminishing the side-peak amplitude. Overall, MT-encoded timestamps could therefore provide a workaround to the side-peak phenomenon. However, since the peaks do not gradually vanish with a higher number of connected channels, but are immediately suppressed by two channels being connected, we suppose that the suppression is most likely due to the reduced signal height.

IV. Discussion

Coincidence experiments with the presented scintillators and SiPMs coupled to the TOFPET2 ASIC evaluation kit resulted in CTRs that are close to or better than state-of-the-art CTRs reported for this and other readout circuits that include a TDC and offer upscaling to the PET system level [13], [28]. Revealing the actual limitations of the CTR due to the scintillator and SiPM, HF SiPM readout featuring digitization via an oscilloscope has shown to achieve CTRs of 60 ps for small LSO:Ce crystals, co-doped with 0.4 % Ca, (2 × 2 × 3 mm^3) and sub-100 ps for larger crystals (LSO:Ce,Ca; 2 × 2 × 20 mm^3) in prior studies [8]. In this study, an LYSO:Ce,Ca crystal (TAC; 2 × 2 × 3 mm^3) achieved a CTR of (73 ± 1) ps, which is comparable to the values reported in literature considering that we used commercially available Broadcom SiPMs with a glass window as opposed to the literature values measured with FBK SiPMs and no protection window [9]. Furthermore, the results shown in Fig. 7 point to a saturated timing performance starting from 3 V overvoltage for HPK SiPMs and from 5 V overvoltage for Broadcom SiPMs. This behavior is mainly linked to the saturation of the SiPMs' photon detection efficiency (PDE) for these overvoltages, as shown in [9].

We have shown the feasibility of applying a similar high-speed amplification before the TOFPET2 ASIC, which leads to improved CTR and single-photon resolution in corresponding staircase plots for all tested SiPMs. However, an additional power consumption of 193 mW per amplified channel could be a true show stopper concerning the system integration of such a circuit. It at least requires a high-power infrastructure as well as efficient cooling strategies to dissipate the heat generated by the electrical components. Further studies on the possibility of replacing the chosen amplifier BGA616, e.g., by the BGA2851 selected for the HF circuitry featuring digitization via an oscilloscope, ought to be conducted in the following. We have investigated that these other types of RF amplifiers, e.g., BGA2851, deliver similar and even better timing performance in measurements with oscilloscope readout, while reducing the power consumption to 35 mW. Additionally, channel compression or multiplexing schemes, such as row–column readout or one timing channel for (sub-)units of detector blocks [29]–[31], could be taken into consideration to reduce the number of amplified, fast-timing channels needed. MTE has a positive effect on the CTR as well, stabilizing the baseline of the ASIC by an effectively reduced input stage impedance. For both amplified readout and MTE, the CTR achieved with standard LYSO:Ce crystals is now close to or even better than values achieved with specially grown calcium co-doped LSO:Ce crystals [13]. With respect to system integration, MTE will require a higher number of ASIC channels for digitization. From Fig. 12, it can be seen that the benefit of connecting more channels is only marginal for $n \geq 3$ channels. Still, investigating channel compression schemes with multiple channels connected to each SiPM in an SiPM array would be of advantage to maintain a low form factor of the integrated electronics and not triple the power consumption per SiPM channel. Regarding the multichannel application of these proposed solutions, the influence of multichannel specific effects such as cross-talk between channels should be characterized as it might lead to a performance degradation.

However, the comparison with the CTRs from measurements conducted with the HF electronics and oscilloscope readout shows that the design of the SiPM front-end readout currently plays a key role in limiting the CTR. None of the presented methods is able to achieve CTRs below 100 ps with the TOFPET2 ASIC, although it has been shown that the crystals (TAC LYSO:Ce,Ca 2 × 2 × 3 mm^3) and SiPMs (Broadcom AFBR-S4N33C013) are capable of a CTR of 73 ps when using HF readout and an oscilloscope. In addition, none

of the obtained results fits the squared addition of the CTR of SiPM and scintillator (CTR_{HF}) and the intrinsic CTR of the ASIC [$CTR_{intrinsic}$, see (1)]. This leads to the conclusion that there has to be another contributor to the CTR of the complete readout chain (scintillator—SiPM—electronic front end—TDC—clock synchronization) that could not yet be identified, but might be linked to the TDC alignment jitter between two different ASICs. For the example of the LYSO:Ce,Ca crystal (TAC; $2 \times 2 \times 3$ mm^3), the CTR deteriorated from (73 ± 1) to (134 ± 10) ps, comparing the HF readout and the TOFPET2 ASIC. Here, adding up the contributions of SiPM and scintillator and the intrinsic timing of the TOFPET2 ASIC [see (1)], i.e., $CTR_{intrinsic} = 58$ ps, would suggest a CTR of 93 ps that should be possible to achieve with the TOFPET2 ASIC. To investigate further contributions to this, e.g., the clock distribution via FEB/D and FEB/I within the evaluation kit, intrinsic measurements with one SiPM channel being connected to two different ASICs on the same or different FEB/Is and FEB/D ports, respectively, are anticipated. This, however, is currently limited by noise pickup and the connection of two FEB/A grounds via the SiPM cathode. A possible alternative would be laser-based irradiation of two SiPMs to mimic a scintillator with quasi-infinite light yield and therefore subtract the contribution of this component to the timing performance. Another important measurement to assess further contributions to the CTR is a coincidence measurement between two SiPMs on the same ASIC. Furthermore, there is a slight difference in CTR between Broadcom and HPK SiPMs if the SiPMs are read out by the HF circuit featuring digitization via an oscilloscope, which then vanishes if the SiPMs are read out by the TOFPET2 ASIC. In this study, we assume that the contribution to the CTR of the scintillators and SiPMs and the contribution of the electronics are uncorrelated for the given type of measurement. It might be that a difference in performance for the case of standard TOFPET2 readout is superposed by the contribution of the electronics and baseline shifts occurring more likely for Broadcom SiPMs with a smaller SPAD size and also a higher DCR. When changing the electronic front end, PZ filters are employed, reducing baseline shifts. Hence, the reported CTR values are slightly better for Broadcom again.

The novel side peaks observed in the coincidence time difference spectra seem to be related to the signal height at the input stage, as their amplitude and also the displayed order are increased with higher SiPM overvoltages and SiPM signal amplification in the case of using an amplifier in front of the ASIC. Since they also appear in measurements assessing the intrinsic timing of the ASIC (see Fig. 8), they have to be related to the electronic front end. As the electronic front end seems to have a problem with higher signal amplitudes that affects the timestamp generation, this could lead to the improved performance of the MTE circuit. However, if MTE can maintain this outcome for amplified signals have to be tested by combining the amplified readout and MTE before the input stage of the TOFPET2 ASIC. This could also help to identify whether the side peaks are generated simultaneously on multiple ASIC channels or whether this is an effect on a channel-individual basis. In TOF-PET, these side peaks can imply a severe problem and will be especially problematic for PET system applications with their spacious source distributions or the imaging of large objects. With default ASIC configuration, up to 40 % of the measured coincidences (energy filter applied) will be affected by the falsely generated timestamps (see Fig. 14). The side peaks are distinguishable from the main peak in benchtop setups with a point source—if the CTR is sufficiently low. Depending on the application and the achieved CTR, the peaks will be superposed by the tails of the coincidence time difference distribution, possibly contributing to a worse CTR. In this situation and with the default setup, the user currently has no means at hand to identify whether the CTR is caused by the hardware configuration or by the generation of the side peaks. Generating multiple timestamps per event, as done in MTE, might be a means to detect or prevent the side-peak generation—assuming that the peaks are not generated equally on different channels. Two timestamps per SiPM channel would at least be necessary and would in addition allow for correcting the time walk based on the rise time if configured with different thresholds, e.g., for BGO scintillators [32]. This might also flag the appearance of the satellite peaks characterized in [14] due to a longer signal rise time. However, to enable at least two or even more TDCs per SiPM channel in a PET system, electronic multiplexing schemes need to be developed that keep the number of required channels at a minimum. Another possibility is a redesign of the ASIC to generate two timestamps in the timing branch, one by each already present discriminator. To overcome the bandwidth limitation of the input stage, also modifications of the input stage will be necessary. Here, it is in question, whether the power consumption of the TOFPET2 ASIC, which is currently very low and therefore beneficial for system-level applications [15], can be maintained.

V. Conclusion and Outlook

This study has shown that the TOFPET2 ASIC can achieve sub-200 ps timing with typical scintillator thickness used in clinical systems (e.g., $3 \times 3 \times 20$ mm^3). The introduced external front-end modifications have shown to boost the timing performance of the TOFPET2 ASIC, but have not reached the desired CTR of 100 ps, which the ASIC should be capable of, assuming a quadratic addition of the contribution of the SiPM and crystal and the intrinsic CTR of the front end and TDC. Future investigations will consider measuring the jitter of the clock between two FEB/I boards and two FEB/D ports, respectively. The newly observed side peaks reveal that the ASIC input stage does not respond well to higher signal amplitudes. In this view, the TOFPET2 ASIC is still suited for high-performance TOF-PET measurements, but requires some improvements for the next-generation 100-ps PET systems which are sought by the community now. It is of further interest, whether the sub-200 ps CTR can be maintained with a detector matrix. For ultrafast timing applications, we have revealed that the input stage of the ASIC probably poses the main problem to this behavior and most likely needs to be redesigned to keep up with state-of-the-art analog SiPMs.

ACKNOWLEDGMENT

The authors declare the following financial interests/personal relationships which may be considered as potential competing interests with the work reported in this article: V.S., D.S., and B.W., are co-founders and employees of the spin-off company Hyperion Hybrid Imaging Systems GmbH, Aachen, Germany. The authors would like to thank Stefan Brunner from Broadcom for providing SiPM samples. The authors would also like to thank Mitch Chou from National Sun Yat-sen University and Jack Lin from TACs for providing the LYSO:Ce,Ca samples. Furthermore, the authors would like to thank Stefan Tavernier, Ricardo Bugalho, and Luis Ferramacho from PETsys Electronics S.A. for sharing their expertise in their many discussions.

REFERENCES

[1] S. Surti, "Update on time-of-flight PET imaging," *J. Nucl. Med.*, vol. 56, no. 1, pp. 98–105, 2015, doi: 10.2967/jnumed.114.145029.

[2] D. Bharkhada, L. Eriksson, M. Conti, and H. Rothfuss, "SNR TOF gain in high time resolution PET systems," in *Proc. IEEE Nucl. Sci. Symp. Med. Imag. Conf. (NSS/MIC)*, 2017, pp. 1–2, doi: 10.1109/NSSMIC.2017.8532785.

[3] D. R. Schaart, G. Schramm, J. Nuyts, and S. Surti, "Time of flight in perspective: Instrumental and computational aspects of time resolution in positron emission tomography," *IEEE Trans. Radiat. Plasma Med. Sci.*, vol. 5, no. 5, pp. 598–618, Sep. 2021, doi: 10.1109/TRPMS.2021.3084539.

[4] S. Surti and J. S. Karp, "Update on latest advances in time-of-flight PET," *Physica Medica*, vol. 80, pp. 251–258, Dec. 2020, doi: 10.1016/j.ejmp.2020.10.031.

[5] S. Gundacker and A. Heering, "The silicon photomultiplier: Fundamentals and applications of a modern solid-state photon detector," *Phys. Med. Biol.*, vol. 65, no. 17, Aug. 2020, Art. no. 17TR01, doi: 10.1088/1361-6560/ab7b2d.

[6] M. Nemallapudi, S. Gundacker, P. Lecoq, and E. Auffray, "Single photon time resolution of state of the art SiPMs," *J. Instrum.*, vol. 11, no. 10, pp. P10016–P10016, Oct. 2016, doi: 10.1088/1748-0221/11/10/p10016.

[7] J. W. Cates, S. Gundacker, E. Auffray, P. Lecoq, and C. S. Levin, "Improved single photon time resolution for analog SiPMs with front end readout that reduces influence of electronic noise," *Phys. Med. Biol.*, vol. 63, no. 18, Sep. 2018, Art. no. 185022, doi: 10.1088/1361-6560/aadbcd.

[8] S. Gundacker, R. M. Turtos, E. Auffray, M. Paganoni, and P. Lecoq, "High-frequency SiPM readout advances measured coincidence time resolution limits in TOF-PET," *Phys. Med. Biol.*, vol. 64, no. 5, Feb. 2019, Art. no. 055012, doi: 10.1088/1361-6560/aafd52.

[9] S. Gundacker *et al.*, "Experimental time resolution limits of modern SiPMs and TOF-PET detectors exploring different scintillators and Cherenkov emission," *Phys. Med. Biol.*, vol. 65, no. 2, Jan. 2020, Art. no. 025001, doi: 10.1088/1361-6560/ab63b4.

[10] M. Miyata, H. Tomita, K. Watanabe, J. Kawarabayashi, and T. Iguchi, "Development of TOF-PET using Cherenkov radiation," *J. Nucl. Sci. Technol.*, vol. 43, no. 4, pp. 339–343, 2006, doi: 10.1080/18811248.2006.9711101.

[11] N. Kratochwil, S. Gundacker, P. Lecoq, and E. Auffray, "Pushing Cherenkov PET with BGO via coincidence time resolution classification and correction," *Phys. Med. Biol.*, vol. 65, no. 11, Jun. 2020, Art. no. 115004. doi: 10.1088/1361-6560/ab87f9.

[12] R. H. Pots, E. Auffray, and S. Gundacker, "Exploiting cross-luminescence in BAF2 for ultrafast timing applications using deep-ultraviolet sensitive HPK silicon photomultipliers," *Front. Phys.*, vol. 8, p. 482, Oct. 2020, doi: 10.3389/fphy.2020.592875.

[13] R. Bugalho *et al.*, "Experimental characterization of the TOFPET2 ASIC," *J. Instrum.*, vol. 14, no. 3, pp. P03029–P03029, Mar. 2019, doi: 10.1088/1748-0221/14/03/p03029.

[14] D. Schug, V. Nadig, B. Weissler, P. Gebhardt, and V. Schulz, "Initial measurements with the PETsys TOFPET2 ASIC evaluation kit and a characterization of the ASIC TDC," *IEEE Trans. Radiat. Plasma Med. Sci.*, vol. 3, no. 4, pp. 444–453, Jul. 2019, doi: 10.1109/TRPMS.2018.2884564.

[15] V. Nadig, B. Weissler, H. Radermacher, V. Schulz, and D. Schug, "Investigation of the power consumption of the PETsys TOFPET2 ASIC," *IEEE Trans. Radiat. Plasma Med. Sci.*, vol. 4, no. 3, pp. 378–388, May 2020, doi: 10.1109/TRPMS.2019.2955032.

[16] V. Nadig, D. Schug, B. Weissler, and V. Schulz, "Evaluation of the PETsys TOFPET2 ASIC in multi-channel coincidence experiments," *EJNMMI Phys.*, vol. 8, no. 1, pp. 1–21, 2021, doi: 10.1186/s40658-021-00370-x.

[17] M. Li, B. Yockey, and S. Abbaszadeh, "Design study of a dedicated head and neck cancer PET system," *IEEE Trans. Radiat. Plasma Med. Sci.*, vol. 4, no. 4, pp. 489–497, Jul. 2020, doi: 10.1109/TRPMS.2020.2964293.

[18] M. Li and S. Abbaszadeh, "Depth-of-interaction study of a dual-readout detector based on TOFPET2 application-specific integrated circuit," *Phys. Med. Biol.*, vol. 64, no. 17, Sep. 2020, Art. no. 175008, doi: 10.1088/1361-6560/ab3866.

[19] E. Lamprou, A. J. Gonzalez, F. Sanchez, and J. M. Benlloch, "Exploring TOF capabilities of PET detector blocks based on large monolithic crystals and analog SiPMs," *Physica Medica*, vol. 70, pp. 10–18, Oct. 2020, doi: 10.1016/j.ejmp.2019.12.004.

[20] K. Park, J. Jung, Y. Choi, H. Leem, and Y. Kim, "Feasibility study of a time-of-flight brain positron emission tomography employing individual channel readout electronics," *Sensors*, vol. 21, no. 6, p. 5566, 2021, doi: 10.3390/s21165566.

[21] M. Wang, Y. Wang, and L. Wang, "Evaluation of high-resolution and depth-encoding PET detector modules based on single-ended readout with TOFPET2 ASIC," *Radiat. Detect. Technol. Methods*, vol. 5, no. 3, pp. 451–458, 2021, doi: 10.1007/s41605-021-00270-9.

[22] A. Gola, C. Piemonte, and A. Tarolli, "Analog circuit for timing measurements with large area SiPMs coupled to LYSO crystals," *IEEE Trans. Nucl. Sci.*, vol. 60, no. 2, pp. 1296–1302, Apr. 2013. [Online]. Available: https://ieeexplore.ieee.org/document/6154091

[23] S. Gundacker *et al.*, "A systematic study to optimize SiPM photo-detectors for highest time resolution in PET," *IEEE Trans. Nucl. Sci.*, vol. 59, no. 5, pp. 1798–1804, Oct. 2012, doi: 10.1109/TNS.2012.2202918.

[24] A. LaBella, S. Tavernier, C. Woody, M. Purschke, W. Zhao, and A. H. Goldan, "Toward 100 ps coincidence time resolution using multiple timestamps in depth-encoding PET modules: A Monte Carlo simulation study," *IEEE Trans. Radiat. Plasma Med. Sci.*, vol. 5, no. 5, pp. 679–686, Sep. 2021, doi: 10.1109/TRPMS.2020.3043691.

[25] S. Mandai and E. Charbon, "A $4 \times 4 \times 416$ digital SiPM array with 192 TDCs for multiple high-resolution timestamp acquisition," *J. Instrum.*, vol. 8, no. 5, pp. P05024–P05024, May 2013, doi: 10.1088/1748-0221/8/05/p05024.

[26] L. H. C. Braga, L. Gasparini, and D. Stoppa, "A time of arrival estimator based on multiple timestamps for digital PET detectors," in *Proc. IEEE Nucl. Sci. Symp. Med. Imag. Conf. Rec. (NSS/MIC)*, 2012, pp. 1250–1252, doi: 10.1109/NSSMIC.2012.6551306.

[27] S. M. Qaisar, "A two stage interpolator and multi threshold discriminator for the brain-pet scanner timestamp calculation," *Nucl. Instrum. Methods Phys. Res. A, Accelerators Spectrometers Detectors Assoc. Equip.*, vol. 922, pp. 364–372, Apr. 2019, doi: 10.1016/j.nima.2019.01.004.

[28] V. Stankova *et al.*, "STIC3—Silicon photomultiplier timing chip with picosecond resolution," *Nucl. Instrum. Methods Phys. Res. A, Accelerators Spectrometers Detectors Assoc. Equip.*, vol. 787, pp. 284–287, Jul. 2015, doi: 10.1016/j.nima.2014.12.073.

[29] S. Dey, E. Myers, T. K. Lewellen, R. S. Miyaoka, and J. C. Rudell, "A row-column summing readout architecture for SiPM based PET imaging systems," in *Proc. IEEE Nucl. Sci. Symp. Med. Imag. Conf. (NSS/MIC)*, 2013, pp. 1–5, doi: 10.1109/NSSMIC.2013.6829062.

[30] P. Fan, T. Xu, Z. Lyu, S. Wang, Y. Liu, and T. Ma, "3D positioning and readout channel number compression methods for monolithic PET detector," in *Proc. IEEE Nucl. Sci. Symp. Med. Imag. Conf. Room-Temperature Semicond. Detect. Workshop (NSS/MIC/RTSD)*, 2016, pp. 1–4, doi: 10.1109/NSSMIC.2016.8069404.

[31] J. Y. Won *et al.*, "Development and initial results of a brain PET insert for simultaneous 7-Tesla PET/MRI using an FPGA-only signal digitization method," *IEEE Trans. Med. Imag.*, vol. 40, no. 6, pp. 1579–1590, Jun. 2021, doi: 10.1109/TMI.2021.3062066.

[32] N. Kratochwil, E. Auffray, and S. Gundacker, "Exploring Cherenkov emission of BGO for TOF-PET," *IEEE Trans. Radiat. Plasma Med. Sci.*, vol. 5, no. 5, pp. 619–629, Sep. 2021, doi: 10.1109/TRPMS.2020.3030483.